Journal of Biomedical Optics

BiomedicalOptics.SPIEDigitalLibrary.org

FRET efficiency measurement in a molecular tension probe with a low-cost frequency-domain fluorescence lifetime imaging microscope

John-Paul Dumas
James Y. Jiang
Evan M. Gates
Brenton D. Hoffman
Mark C. Pierce
Nada N. Boustany

John-Paul Dumas, James Y. Jiang, Evan M. Gates, Brenton D. Hoffman, Mark C. Pierce, Nada N. Boustany, "FRET efficiency measurement in a molecular tension probe with a low-cost frequency-domain fluorescence lifetime imaging microscope," *J. Biomed. Opt.* **24**(12), 126501 (2019), doi: 10.1117/1.JBO.24.12.126501.

Journal of Biomedical Optics 24(12), 126501 (December 2019)

FRET efficiency measurement in a molecular tension probe with a low-cost frequency-domain fluorescence lifetime imaging microscope

John-Paul Dumas,[a,b,†] James Y. Jiang,[b,†] Evan M. Gates,[c] Brenton D. Hoffman,[c] Mark C. Pierce,[a] and Nada N. Boustany[a,*]
[a]Rutgers University, Department of Biomedical Engineering, Piscataway, New Jersey, United States
[b]Thorlabs Inc., Newton, New Jersey, United States
[c]Duke University, Department of Biomedical Engineering, Durham, North Carolina, United States

Abstract. We demonstrate the possibility of measuring FRET efficiency with a low-cost frequency-domain fluorescence lifetime imaging microscope (FD-FLIM). The system utilizes single-frequency-modulated excitation, which enables the use of cost-effective laser sources and electronics, simplification of data acquisition and analysis, and a dual-channel detection capability. Following calibration with coumarin 6, we measured the apparent donor lifetime in mTFP1-mVenus FRET standards expressed in living cells. We evaluated the system's sensitivity by differentiating the short and long lifetimes of mTFP1 corresponding to the known standards' high and low FRET efficiency, respectively. Furthermore, we show that the lifetime of the vinculin tension sensor, VinTS, at focal adhesions (2.30 ± 0.16 ns) is significantly ($p < 10^{-6}$) longer than the lifetime of the unloaded TSMod probe (2.02 ± 0.16 ns). The pixel dwell time was 6.8 μs for samples expressing the FRET standards, with signal typically an order of magnitude higher than VinTS. The apparent FRET efficiency ($E_{\mathrm{FRET}}^{\mathrm{app}}$) of the standards, calculated from the measured apparent lifetime, was linearly related to their known FRET efficiency by a factor of 0.92 to 0.99 ($R^2 = 0.98$). This relationship serves as a calibration curve to convert apparent FRET to true FRET and circumvent the need to measure multiexponential lifetime decays. This approach yielded a FRET efficiency of 18% to 19.5%, for VinTS, in agreement with published values. Taken together, our results demonstrate a cost-effective, fast, and sensitive FD-FLIM approach with the potential to facilitate applications of FLIM in mechanobiology and FRET-based biosensing. [DOI: 10.1117/1.JBO.24.12.126501]

Keywords: fluorescence lifetime imaging microscope; fluorescence resonance energy transfer; frequency domain; molecular tension probes; vinculin tension sensor.

Paper 190249RR received Jul. 12, 2019; accepted for publication Nov. 11, 2019; published online Dec. 28, 2019.

1 Introduction

The role of mechanotransduction in biology has been extensively reviewed and points to a significant and central role played by mechanical forces and the cytoskeleton in shaping cellular function and behavior.[1–4] The potential to control complex cellular function by understanding mechanotransduction has important implications for the design of therapeutic strategies in many pathological conditions, including degenerative diseases and injury, cancer, and aging.

While the subcellular localization of adhesion molecules and the architecture of focal adhesions can be imaged by conventional and by super-resolution fluorescence microscopy,[5,6] actual tension measurements require techniques that are sensitive to piconewton level forces at the cellular and subcellular scales. To this end, fluorescence resonance energy transfer (FRET) probes consisting of molecular springs inserted between a fluorescent donor and acceptor pair have been the focus of much recent interest. Changes in molecular tension are measured by quantifying changes in the FRET signal between the donor and acceptor.[7–9] Intramolecular tension-sensing fluorescent probes have been demonstrated,[10,11] where an elastic linker module flanked by an FRET donor and acceptor pair is inserted into a load-bearing protein using recombinant DNA methods. Unlike FRET biosensors that toggle between a high and low FRET state, these FRET tension probes are expected to report on a nonbinary, spatiotemporal intracellular distribution of mechanical load. Thus, the ability to quantify accurately their FRET efficiency presents a challenge for microscopic imaging.

A sensitive and direct method to measure changes in FRET signal relies on measuring the donor's fluorescence lifetime in the presence of the acceptor (τ_{DA}), relative to the donor's lifetime in the absence of the acceptor (τ_D).[12] Thus, FRET imaging can be achieved via fluorescence lifetime imaging microscopy (FLIM), using only measurements within the donor's spectral emission channel. Fluorescence lifetime is largely independent of fluorophore concentration, and with selection of appropriate spectral filters, the donor channel can be made free of cross-talk signal from the acceptor. Using this FLIM-FRET approach, fluorescent donors can even be coupled with nonfluorescent acceptors, expanding the range of viable donor-quencher pairs. However, the donor and acceptor fluorophores in FRET sensors are typically separated by a flexible linker, giving rise to fluorescence emission decays with multiple time constants. Thus, FLIM systems designed to measure FRET typically rely on

*Address all correspondence to Nada N. Boustany, E-mail: nboustan@soe.rutgers.edu

†These authors contributed equally to this work.

resolving multiexponential decays and then calculating FRET efficiency from the amplitude-weighted average lifetime.[12]

Two approaches to FLIM may be implemented for FRET applications. Time-domain (TD) FLIM consists of measuring the fluorescence signal decay as a function of time after exciting the sample with a very short laser pulse. On the other hand, frequency-domain (FD) FLIM consists of measuring fluorescence lifetime by measuring the modulation and phase of the fluorescence emission excited by a frequency-modulated laser source. Both of these approaches have been extensively reviewed in the literature and are utilized in numerous applications ranging from metabolic imaging to protein conformation and protein interaction.[12–15] Recent developments in FLIM technology have also given rise to approaches for achieving high speed depth-resolved,[16–19] widefield,[20–23] and multichannel[24] FLIM. For example, Bower et al. recently demonstrated a state-of-the-art high-speed FLIM system using a mode-locked pulsed Ti: Sapphire laser synchronized with a 1.8-GS/s digitizer to directly sample the fluorescence decay signal and analyze it by a single exponential fit, with temporal resolution only limited by the sampling rate of the digitizer.[16] Commercially available FLIM systems include highly sensitive frequency-domain fluorescence lifetime imaging microscope (FD-FLIM) systems (for example, ISS Inc, Lambert Instruments BV) operating at multiple modulation frequencies or phases, as well as TD-FLIM systems that rely on time-correlated single photon counting (for example, Becker and Hickl GmbH, Picoquant GmbH, Leica Microsystems, Inc). These highly sensitive systems are capable of accurately measuring multiexponential lifetimes, which are expected for FRET probes within living cells such as the tension probe investigated here. In addition, FD-FLIM systems operating at multiple modulation frequencies allow for approaches such as the polar, or phasor, plots for analysis of complex multiexponential lifetimes.[19,25] However, current barriers to adopting FLIM to quantify FRET efficiency still exist due to the high cost of pulsed laser sources, the potential complexity of data acquisition and analysis, and the relatively slow imaging speed of FLIM in weakly fluorescent samples, requiring long integration times to accurately resolve multiexponential decays. The use of femtosecond-pulsed laser sources combined with multi-GHz digitizers and the need for multiple excitation and emission channels also result in a multiplicative growth of system cost and complexity.

In this paper, we implement a simplified FD-FLIM imaging system for FRET applications. The system is based on the instrument described by Booth and Wilson.[26] The system relies on measuring, at a single modulation frequency, the apparent lifetime of a fluorophore and its corresponding apparent FRET efficiency. Instead of resolving and measuring multiple exponential decays, we use a FRET standards calibration curve to convert the measured apparent FRET efficiency to true FRET efficiency. This approach allows us to utilize sinusoidally modulated laser diodes at single modulation frequencies for fluorescence excitation, and signal processing techniques based on the discrete Fourier transform to implement FD-FLIM in a cost-effective, modular format, which has several advantages. Laser diodes are available at many excitation wavelengths relevant for many fluorescence samples, and they are relatively inexpensive compared with the pulsed laser sources utilized in commercial FLIM systems. Many diodes can be directly intensity modulated at tens to hundreds of MHz using a bias-T modulation circuit by a voltage signal generated by an arbitrary waveform generator. The Fourier transform used for signal processing can achieve phase measurements with much higher accuracy than the 2π time period of a modulated signal. Thus, subnanosecond time resolution can be obtained when modulating a laser in the 20- to 50-MHz range. To generate and measure signals in this frequency range, the Nyquist sampling theory allows the use of electronics with bandwidth on the order of 50 MHz and data converters and sampling rate on the order of 100 MHz. This significantly reduces the cost of the data acquisition hardware compared to the electronics operating in the GHz range in current state-of-the-art high speed FLIM systems. Digitizers are used to measure directly the photon current of highly sensitive PMTs and avoid the photon "pile-up" problem, which may arise when multiple photons arrive at the same time while detecting fluorescence signals with PMTs operating in the single photon-counting regime. This in turn helps improve total optical throughput and the measurement dynamic range of the system. Finally, the fluorescence emission signal may be split spectrally by optical filters toward different detectors, each acting as an analog input channel. The Fourier transform applied to these multiple input channels allows phase measurements at all modulation frequencies (and therefore excitation wavelengths) simultaneously, and the processes are identical on different emission wavelength channels.

We evaluate the system's performance by measuring the apparent lifetime of mTFP1 in mTFP1-mVenus constructs with known high and low FRET efficiency. We show that the FRET efficiency ($E_{\mathrm{FRET}}^{\mathrm{app}}$) estimated based on the apparent lifetime can be related by a linear fit to the known true E_{FRET} of the constructs. This relationship is then used as a standard-based E_{FRET} calibration curve to convert an unknown sample's apparent FRET efficiency measured with our system to its true FRET efficiency. Utilizing this method, we further demonstrate measurements of FRET efficiency in the vinculin tension probe, VinTS[10] at focal adhesions. The use of a single modulation frequency along with the known standards for E_{FRET} calibration allows us to utilize the apparent lifetime measured at a single modulation frequency to infer FRET efficiency and circumvent the need for using multiple modulation frequencies or measuring multiple exponential decays. This approach provides a cost-effective, fast imaging system that can facilitate FLIM in fields, including mechanobiology, which already involve the preparation of FRET constructs similar to the FRET standards needed for our calibration. While current FLIM systems are capable of providing robust platforms for FRET efficiency measurements, a cost-effective, modular, table-top system would also facilitate FLIM applications such as FRET biosensor development in laboratory settings with limited microscopy resources.

2 Methods

2.1 *Optical Setup*

The schematic of the FD fluorescence lifetime imaging system optimized for measurement of FRET between mTFP1 and mVenus is shown in Fig. 1(a). A 450-nm laser diode (LD1) and a 520-nm laser diode (LD2) are used as the excitation light sources. Two pinhole apertures (PH1 and PH2) of 300 μm diameter are placed in front of each laser diode as simple spatial light modulators to transform the elliptically shaped laser diode output into circular beams. Lenses L1 and L2 are used for collimation, generating two beams each with a diameter of about 5 mm. These collimated beams are combined by a dichroic filter

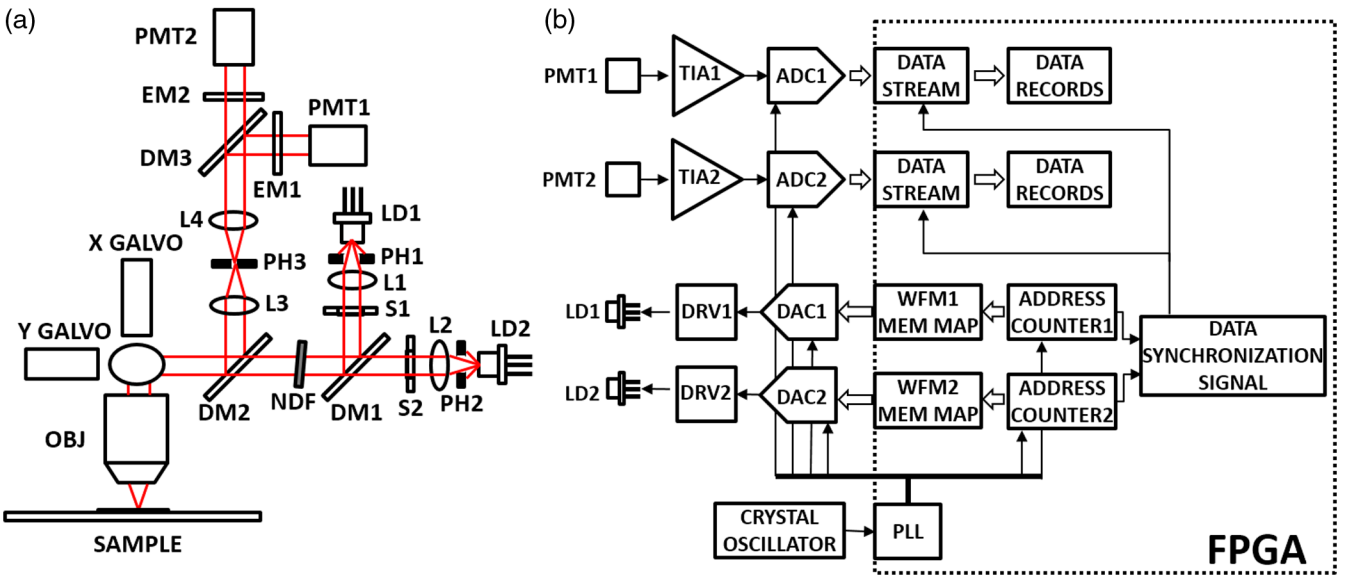

Fig. 1 (a) Optical setup, (b) generation of modulation waveforms and data synchronization signal with minimum phase jitter. LD1, PL450B (Thorlabs); LD2, L520P50 (Thorlabs); PH1, P300D (Thorlabs); PH2, P300D (Thorlabs); L1, AC127-030-A (Thorlabs); L2, AC080-020-A (Thorlabs); S1,S2, SM1SH1 (Thorlabs); DM1, MD480 (Thorlabs); NDF, ND20A (Thorlabs); DM2, Di01-T457/514/647 (Semrock); XY GALVO, GVS202 (Thorlabs); OBJ, 60X/0.85 plan fluorite objective (Nikon) or 60X/1.30 oil objective (Nikon); L3, AC080-016-A (Thorlabs); PH3, P5D (Thorlabs); L4, AC080-016-A (Thorlabs); DM3, DMLP505 (Thorlabs); EM1, MF479-40 (Thorlabs); EM2, MF559-34 (Thorlabs); PMT1,PMT2, PMT2101 (Thorlabs).

(DM1) into a common beam path and are directed toward an optical scan-head consisting of XY galvanometer scanners mounted near the back aperture of an objective lens (OBJ). Two objective lenses were used for this study: a Nikon 0.85 NA/60× dry objective and a Nikon 1.3 NA/60× oil immersion objective. The optical power at the sample did not exceed 25 μW within the scanned point. A multiedge excitation filter (DM2) transmits the two excitation wavelengths and reflects the fluorescent emissions toward a 10-μm confocal pinhole (PH3). Another dichroic filter (DM3) separates the fluorescent emissions into two wavelength bands, subsequently filtered by two emission filters (EM1 and EM2) placed before two photomultiplier tube detectors (PMT1 and PMT2). The excitation and emission spectra of mTFP1 and mVenus along with the filter transmission curves are shown in Fig. S1 in the Supplementary Material.

2.2 *Electronics and Signal Processing*

Figure 1(b) shows the electronics signal chain connected to the lasers and detectors in Fig. 1(a). Using one laser (LD1) as an example, its driver (DRV1) provides a DC bias current and temperature stabilization for this laser. A sinusoidal waveform generated from a digital-to-analog converter (DAC1) is provided to the laser driver to modulate the output intensity of the laser via a bias-T circuit inside the laser driver. On the detection side, the output of a photomultiplier tube (PMT1) is amplified by a transimpedance amplifier (TIA1) and digitized by an analog-to-digital converter (ADC1) to generate a digital data stream for subsequent processing. We show the excitation and emission waveforms (Figs. S2–S5 in the Supplementary Material) and provide additional detail about the electronics in Note #2 in the Supplemental Material. In a frequency domain FLIM system, the fluorescence lifetime is calculated from the measured phase of the emission signals. Therefore, it is critical to minimize the phase noise between the generation of modulation signals and the detection of emission signals. The generation of multiple modulation waveforms also needs to be synchronized with the detection of multiple emission signals. This synchronization process is performed in the digital domain of the system using a field-programmable gate array (FPGA) chip. A 50-MHz crystal oscillator is used as the only clock source in the system. A phase-locked loop inside the FPGA chip generates one master clock ($f_{\mathrm{CLK}} = 150$ MHz) based on the crystal oscillator input, which is then used for timing of all counters and data converters within the system. The generation of the laser modulation waveform is based on the direct digital synthesis (DDS) method used in modern arbitrary waveform generators.[27] In DDS, the output of the memory map feeds the input of the digital-to-analog converter, and its memory read address is updated by a counter (ADDRESS COUNTER1). The frequency of the laser modulation waveform is determined by the update rate of the address counter:

$$f_{\mathrm{mod}} = R = \frac{f_{\mathrm{CLK}}}{(l/s)}, \tag{1}$$

where f_{mod} is the modulation frequency of the laser, R is the update rate of the address counter. f_{CLK} is the clock frequency at which the address counter is working. l is the length of the waveform memory map where one complete modulation waveform is stored and s is the increment step size of the address counter. l and s are both integers.

Since two modulation waveforms of different frequencies are required (one for each laser diode), we choose different step sizes for the two address counters responsible for each waveform:

$$a_1 s_1 = a_2 s_2 = bl, \tag{2}$$

where s_1 and s_2 are the step sizes for the two address counters and a is the number of counting events that two counters can coincide to produce a data synchronization signal. In our system, $f_{\mathrm{CLK}} = 150$ MHz, $l = 8192$, $s_1 = 2304$, $s_2 = 5260$, $a_1 = 160$, $a_2 = 144$, and $b = 45$. The frequencies of the modulation waveforms for the 450-nm laser (f_1) and 520-nm laser (f_2) are 42.1875 and 46.8750 MHz, respectively.

Using the above parameters, a synchronization signal is generated when 160 cycles of waveform 1 and 144 cycles of waveform 2 are generated in the same time period and when the two address counters coincide in values. This data synchronization signal is used as the acquisition trigger signal for the two analog-to-digital converters to organize the data stream into multiple data records. Each data record contains the intensity-modulated fluorescence emission signals time-aligned to the acquisition trigger signal and can be used for data processing and analysis.

A fast Fourier transform (FFT) is performed on each acquired data record to calculate the magnitude and phase of the emission signals at multiple modulation frequencies simultaneously. Since the laser excitation wavelengths are frequency encoded at f_1 and f_2, and the emission signals are optically split into PMT1 and PMT2, the system is therefore capable of measuring fluorescence lifetime simultaneously from two fluorophores whose detection channels are segregated by the choice of modulation frequencies, and appropriate dichroic mirror and bandpass filters (see Note #3 and Fig. S6 in the Supplementary Material).

The discrete Fourier transform of the signals $u(t)$ from a detector can be written as[28]

$$u(t) = \frac{A_0}{2} + \sum_{n=1}^{N-1} M_n \cos(\omega_n t - \phi_n), \tag{3}$$

where M_n and ϕ_n are the magnitude and phase angle of the n'th frequency component:

$$M_n = \sqrt{A_n^2 + B_n^2}, \tag{4}$$

$$\phi_n = \arctan\frac{B_n}{A_n}. \tag{5}$$

Here, $A_n = M_n \cos\phi_n$ and $B_n = M_n \sin\phi_n$ are the real and imaginary parts of the n'th frequency component in the Fourier transformed data. ω_n is the angular frequency of the n'th frequency component and N is the half value of the FFT window length:

$$\omega_n = 2\pi f_n = \pi n \frac{f_{\mathrm{clk}}}{N}. \tag{6}$$

In our system, f_{clk} is the sampling frequency of the A/D converters at 150 MHz. The point integration time can be adjusted by changing the lengths of raw data points acquired at each sample location, which also changes the window length in the FFT calculation. For example, when a data record length and FFT window length are both chosen to be 1024, the integration time at each measurement point is 6.83 μs. This integration time can be selected between 1.27 and 109.28 μs in seven steps by successively doubling the data acquisition length for FFT calculation.

The signal processing and system control software is written in C++ and Visual Basic. The software configures the frequency, amplitude, and phase of the laser modulation signals and processes the digitized waveforms from the detectors to measure the magnitude and phase angle at each sample location. The magnitude information is used to construct an intensity image, and the phase information is used to construct a lifetime image of the sample.

2.3 *Calculation and Calibration of Lifetime*

In our FD FLIM system, the sample is illuminated by two intensity modulated light sources of different wavelengths (λ_n) at different frequencies (ω_n), each with a modulation depth of nearly 100%. The intensity of the excitation light can be written as

$$I_{\mathrm{EX}} = \sum_{n=1}^{M} I_{\mathrm{EX}_n}(\lambda_n)\left[\frac{1}{2} + \frac{1}{2}\cos(\omega_n t + \phi_{\mathrm{EX}_n})\right], \tag{7}$$

where $M = 2$ is the number of modulated light sources and I_{EX_n} is the maximum excitation intensity of the n'th light source, modulated at an angular frequency ω_n with an initial phase of ϕ_{EX_n}. The intensity of the fluorescence emission signals can then be written as

$$I_{\mathrm{EM}} = \sum_{n=1}^{M} I_{\mathrm{EM}_n}\left[\frac{1}{2m} + \frac{1}{2}\cos(\omega_n t + \phi_{\mathrm{EM}_n})\right], \tag{8}$$

where I_{EM_n} is the modulated fluorescence intensity, ϕ_{EM_n} is the phase measured at the modulation frequency ω_n, and both are attributed to the n'th light source. m is the relative modulation depth between emission and excitation and corresponds to the reduction of modulation depth of the fluorescence emission compared to the excitation because $m < 1$.

The lifetime of a sample is calculated from the measured phase delay between fluorescence emission and excitation

$$\tau_n = \frac{1}{\omega_n}\tan(\phi_{\mathrm{EM}_n} - \phi_{\mathrm{EX}_n}). \tag{9}$$

In our system, the measured phase delay of the fluorescence signals includes the phase delay introduced by the sample ($\Delta\phi_{\mathrm{sample}}$), combined with the phase delay ($\Delta\phi_{\mathrm{system}}$) introduced by the system, such as the optical path between the sample and detector, and electrical cables between the detectors and data acquisition system, which remain constant during one experiment. The sample's fluorescent lifetime τ is calculated only from the sample-induced phase delay $\Delta\phi_{\mathrm{sample}}$ between the laser excitation phase ϕ_{EX} and fluorescence emission phase ϕ_{EM}, excluding the system-induced phase delay ($\Delta\phi_{\mathrm{system}}$):

$$\tau = \frac{1}{\omega}\tan\Delta\phi_{\mathrm{sample}}, \tag{10}$$

where

$$\Delta\phi_{\mathrm{sample}} = \phi_{\mathrm{EM}} - (\phi_{\mathrm{EX}} + \Delta\phi_{\mathrm{system}}). \tag{11}$$

The calibration task consists of measuring the fluorescence emission phase ϕ_{EM} using a fluorescent standard with known lifetime and therefore a known $\Delta\phi_{\mathrm{sample}}$, to determine the phase calibration value $(\phi_{\mathrm{EX}} + \Delta\phi_{\mathrm{system}})$ for the system.

Once determined, this calibration value can be subtracted from all subsequent measurements of unknown samples by the system, to obtain sample-induced phase delays and lifetimes. In our system, the stability of the phase calibration value was measured to be within ±25 ps over a test period of 4 h.

A fluorophore solution of 0.01 mM coumarin-6 in ethanol was used to calibrate the donor channel, and 0.01 mM fluorescein in phosphate-buffered saline (pH 7.4) was used to calibrate the acceptor channel. The lifetimes of coumarin-6 and fluorescein under these solvent conditions at room temperature are 2.5[29] and 4.0 ns,[30] respectively. 16 μL of the solution was placed in a 13-mm-diameter circular well on a glass slide, covered with a coverslip, then imaged with the system.

2.4 *FRET Constructs*

The FRET constructs used here are summarized in Fig. 2. The mTFP1-$(GGSGGS)_2$-mVenus and mTFP1-TRAF-mVenus constructs have been described previously in Ref. 31. VinTS and TSMod (Plasmids 26019 and 26021, respectively) were obtained from Addgene. We also used the fluorescent protein monomers mTFP1 and mVenus to obtain the unquenched donor lifetime and to assess detection channel cross talk, respectively. TRAF, GGS, and TSMod are referred to as "soluble constructs" in this paper as they are expected to freely diffuse through the cytosol.

2.5 *Cell Preparation*

Immortalized baby mouse kidney (iBMK) cells were cultured in 12-well plates on 18-mm diameter No.1 glass coverslips in complete growth medium consisting of high glucose DMEM (Invitrogen cat. #11965) supplemented with 10% fetal bovine serum and 100 U/mL of penicillin and 100 μg/mL of streptomycin (1% pen/strep). The cell cultures were maintained in an incubator at 38°C with an 8.5% CO_2 in air atmosphere as previously described.[32] Prior to imaging, the cells were transfected with the FRET constructs using lipofectamine LTX (Invitrogen) following the manufacturer's protocol. We used 1.25 μg DNA, 1.25 μL PLUS reagent, and 3 μL lipofectamine reagent in 125 μL OptiMEM, for each culture well with cells grown on an 18-mm-diameter coverslip. The cells were incubated with the transfection mixture for 1 to 3 h in OptiMEM medium (Invitrogen) after which the OptiMEM medium was replaced with the complete growth medium described above. The cells were imaged 24 to 72 h after transfection. During imaging, the cells were placed in an imaging medium consisting of a non-CO_2-dependent buffered Leibowitz L15 medium (Invitrogen) supplemented with 10% FBS and 1% pen/strep. The coverslip with attached cells was mounted on a homemade steel plate sealed with vacuum grease and VALAP (1:1:1 ratio of vaseline, lanolin, and paraffin wax). The cells were imaged at room temperature and room air.

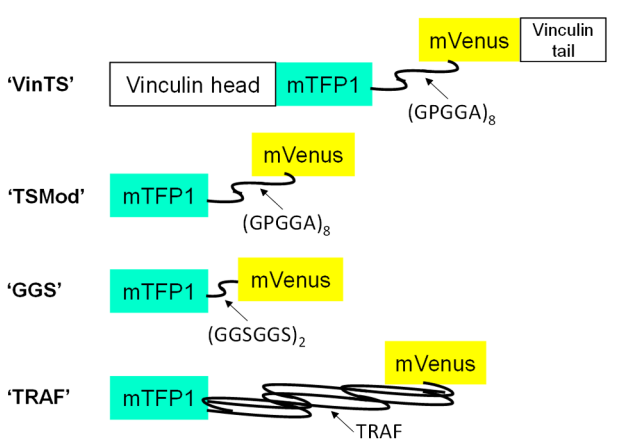

Fluorescent protein construct	Expected FRET efficiency
mTFP1-$(GGSGGS)_2$-mVenus	0.483
mTFP1-TRAF-mVenus	0.053
TSMod	0.286

Fig. 2 FRET constructs with expected FRET efficiency based on the values reported by Gates et al.[31]

2.6 *Image Acquisition and Image Processing*

Intensity and lifetime images were collected in the donor channel (450-nm excitation/479-nm emission band) and, for selected samples, intensity and lifetime images were also collected in the acceptor channel (520-nm excitation/559-nm emission bands). Evaluation of cells expressing mTFP1 revealed that a minimum relative intensity value of 0.01 (1% of maximum) is required for a reproducible lifetime measurement, which corresponds to ~300 photons per pixel (Fig. S7 in the Supplementary Material). Above this value, the measured lifetime is independent of intensity (Fig. S8 in the Supplementary Material). For all data in this report, a minimum relative intensity threshold of 0.01 was used to ensure lifetime measurements were only considered from pixels where there was sufficient fluorescence signal. For display purposes, all pixels with relative intensity values below 0.01 are displayed as black in lifetime images. In addition, pixels measured to have lifetime <0 ns or >5 ns are considered to be a result of phase noise, and these pixels are not included when calculating the average lifetime of a sample.

For the soluble fluorescent constructs, the fluorescence intensity signal was relatively strong. In this case, the raw, unprocessed images were sufficient to extract lifetime information. For weaker samples, such as cells with VinTS expression at focal adhesions, the pixel dwell time was increased to 27.2 μs and 2×2 intensity-weighted pixel binning was applied to lifetime images. For this, the intensity-weighted lifetime within each 2×2 pixel block was calculated by multiplying the lifetime values with their corresponding intensity values at each pixel, then taking the sum and dividing by the sum of the intensities.

The "apparent" lifetime, τ_{DA}^{app}, based on the measured phase delay at a single modulation frequency [Eq. (9)] was used to calculate an apparent FRET efficiency, E_{FRET}^{app}, given as[12]

$$E_{FRET}^{app} = 1 - \frac{\tau_{DA}^{app}}{\tau_D}, \tag{12}$$

where τ_{DA} is the lifetime of the donor (mTFP1) in the presence of acceptor (mVenus), and τ_D is the lifetime of the donor (mTFP1) in the absence of any acceptor. Note: τ_D was measured using samples of cells expressing only mTFP1.

3 Results

3.1 *Lifetime Measurements in Control Constructs*

The measured lifetimes and calculated E_{FRET}^{app} of our fluorescent proteins (mTFP1 and Venus) and our FRET control constructs

[mTFP1-$(GGSGGS)_2$-mVenus and mTFP1-TRAF-mVenus] are shown in Fig. 3. Fluorescence intensity images for each construct are provided for the donor [Figs. 3(a)–3(d)] and acceptor [Figs. 3(e)–3(h)] channels collected with 20 to 25 μW at the sample. For donor-only cells (mTFP1) and acceptor-only cells (mVenus), the fluorescence is isolated to the donor channel and accepter channel, respectively. Importantly, the cross-talk for mVenus to the donor channel is negligible and cannot be distinguished from background noise, indicating that the lifetime measured in the donor channel can be attributed only to donor emission. Fluorescence from cells with the FRET control constructs appears in both the donor and acceptor channels, confirming that both proteins are present in cells after transfection. The corresponding fluorescence lifetime images [Figs. 3(i)–3(l)] are presented for mTFP1 and the FRET control constructs from the donor channel, whereas the mVenus lifetime image is from the acceptor channel.

A blue-to-red color look-up-table is applied to lifetime values for visualization. From this, it is immediately clear that each construct can be distinguished, qualitatively, from the others based on color differences. For quantitative analysis, cells were manually segmented and an intensity-weighted average lifetime was calculated for 145 segmented cells that had a mean relative intensity >0.01. Average lifetime values are 3.071 for mVenus ($n = 40$ cells), 2.845 for mTFP1 ($n = 49$ cells), 2.549 for TRAF ($n = 33$ cells), and 1.515 for $(GGSGGS)_2$ ($n = 23$ cells). These data are displayed in the box and whisker plot in Fig. 3(m) indicating the median (red lines), 25th to 75th percentile (blue boxes), and minimum/maximum (black whiskers) for n number of measured cells. For samples containing the donor, the apparent lifetime was converted to an estimate of FRET efficiency (an apparent FRET) using Eq. (12), which is displayed on the right-hand y axis of Fig. 3(m). While the Venus lifetime is not used to measure the apparent FRET efficiency of the FRET constructs, we include this measurement in Fig. 3(m) to demonstrate the systems' ability to collect lifetime data from two different fluorophores. Figure 3(n) provides a histogram that includes all pixels used to calculate the average lifetime for each cell. The wider distributions of $(GGSGGS)_2$ and TRAF can be attributed to (1) noisier measurements due to weaker signal intensity than cells with mTFP1 or mVenus and (2) the design of the constructs that inherently results in a distribution of FRET efficiency values.

Cells expressing the fluorescent proteins and FRET control constructs were also imaged over a period of time at a high frame rate (128×128 points with a 6.8-μs pixel dwell time for ~9 fps). The lifetime of each construct can be accurately determined at this high frame rate as shown in Fig. 4, where the mean lifetime of cells with each construct is 3.165 ns for mVenus, 2.779 ns for mTFP1, 2.354 ns for TRAF, and 1.551 ns for $(GGSGGS)_2$. These lifetimes are in agreement with the high pixel density data from Fig. 3, being within the limits of cell-to-cell lifetime variation.

The mean intensity and lifetime were measured for a region of interest within a single cell to ensure that photobleaching was minimal. Figure 4 shows the stability of the lifetime data over a period of 120 s (535 frames) when capturing high frame rate images (128×128 pixels). The lifetime of all the samples remained within 2.9% of the initial values after 120 s. For the Nikon 0.85 NA 60× objective and the 450-nm laser diode, the fluence for a single pixel in the 128×128 image is estimated for the diffraction-limited spot with a 6.8-μs pixel dwell time and is

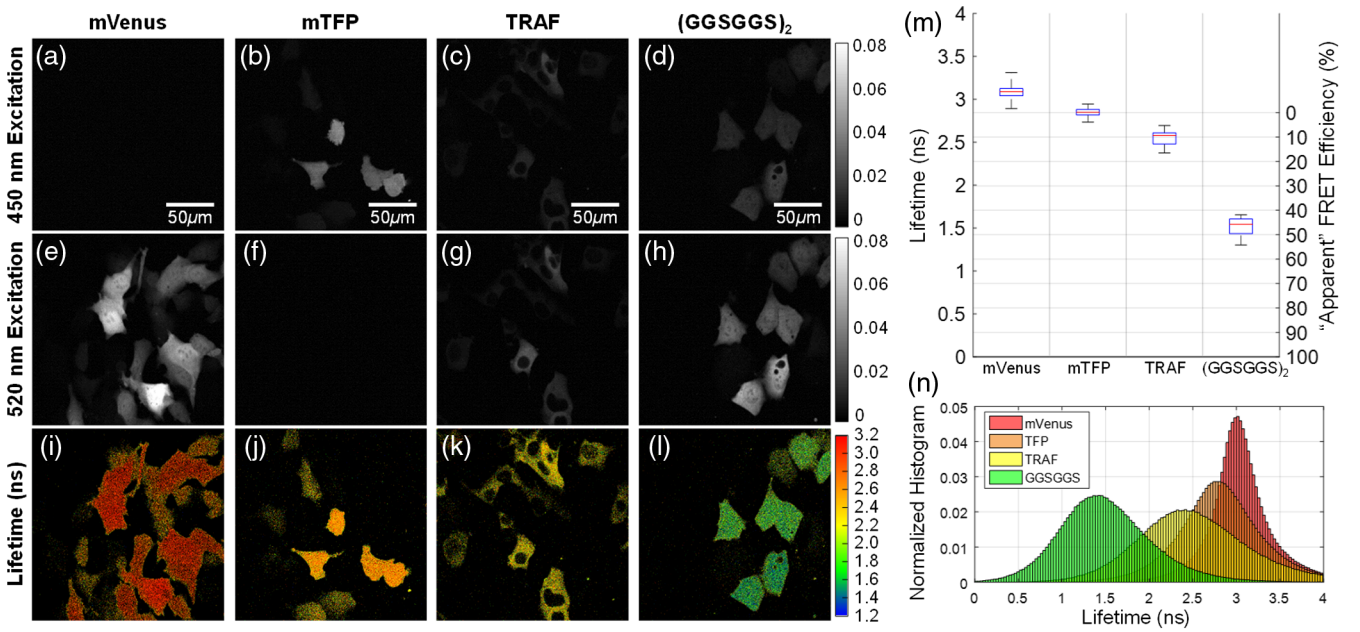

Fig. 3 Representative images of cells with the fluorescent proteins (mVenus and mTFP1) and FRET control constructs [mTFP1-TRAF-mVenus and mTFP1-$(GGSGGS)_2$-mVenus]. (a)–(d) Fluorescence intensity in donor channel (450 nm excitation/479 nm emission band modulated at f_1). (e)–(h) Fluorescence intensity in acceptor channel (520 nm excitation/559 nm emission band modulated at f_2). (i)–(l) Corresponding (i) mVenus and (j)–(l) mTFP1 fluorescence lifetime images. (m) Box and whisker plot for lifetime (left axis) and "apparent" FRET efficiency (right axis). FRET efficiency only applies to samples containing the mTFP1 donor. (n) Normalized histogram of all pixels used to calculate lifetime. All images are captured with 2048×2048 points using the Nikon 0.85 NA 60× objective and a 6.8-μs pixel dwell time.

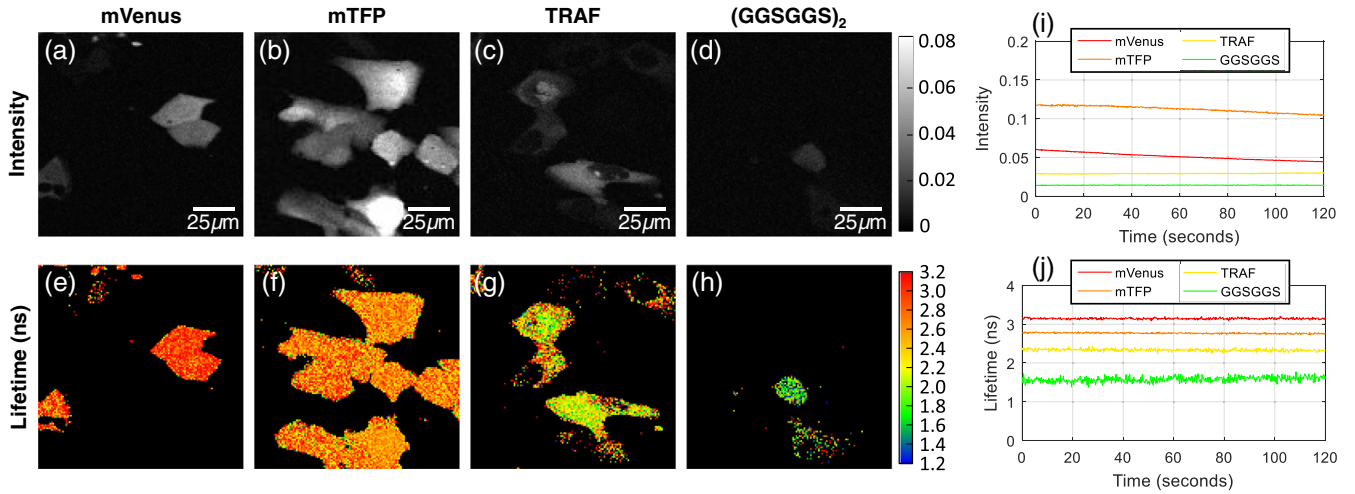

Fig. 4 High-speed imaging and photostability measurements with 25 μW at the sample (Nikon 0.85 NA 60× objective). (a)–(d) Representative intensity images for cells with the fluorescent proteins and control constructs. (e)–(h) Corresponding fluorescence lifetime images. (i) Plots of intensity over time and (j) lifetime over time for a region of interest within a cell. All images are captured with 128 × 128 points at ~9 fps (6.8-μs pixel dwell time). mVenus in (a) is excited with 520 nm and detected within the emission band centered at 559 nm, whereas mTFP, TRAF, and $(GGSGGS)_2$ are excited with 450 nm and detected within the emission band centered at 479 nm.

equal to 0.052 J/cm^2. Over the 120-s measurement, each image pixel is scanned 535 times for a total fluence of 535×0.052 J/cm^2 = 27.8 J/cm^2. The imaging protocol used for data in this report consisted of locating and focusing on cells for no more than 60 s before capturing a high pixel density image, ensuring that images were captured in the regime where photobleaching effects on lifetime measurements are minimal.

3.2 *Lifetime Measurement in the Vinculin Tension Sensor (VinTS)*

To investigate the capabilities of the imaging system in the case of weakly emitting samples that require high-resolution imaging, VinTS was overexpressed in our iBMK cells and its lifetime was compared with that of the unloaded tension module, TSMod. VinTS consists of the elastic tension module TSMod inserted between the head and tail of vinculin.[10] Previous work has demonstrated that VinTS localizes to focal adhesions, similar to vinculin, and bears load at these structures.[10] The expression levels of VinTS in our iBMK cells were significantly lower than those of the soluble constructs. The fluorescence intensity of VinTS was typically an order of magnitude lower than the signal of the soluble FRET constructs including TSMod [see colorbar in Figs. 5(a) and 5(e)]. Focal adhesions are structures on the order of a few microns and require a high resolution objective in order to be properly resolved. For these studies, a Nikon 1.3 NA 40× oil immersion objective was used. 1024 × 1024 pixel images were acquired by scanning over a field of view of width 190 μm. The pixel dwell time was 27.2 μs resulting in ~28 s per frame.

Figure 5 presents example images for TSMod and VinTS samples captured in the donor channel. Cropped regions of the acquired fluorescence intensity images are shown in Figs. 5(a) and 5(e) with their corresponding lifetime images in Figs. 5(b) and 5(f). Processing steps were taken to create pixel masks [Figs. 5(c) and 5(g)] that section only the cells for TSMod samples and only adhesions for VinTS samples. Since fluorescence intensity was weak for VinTS, 2 × 2 intensity-weighted pixel binning was applied to all VinTS and TSMod lifetime images as a means to generate a more accurate lifetime measurement per pixel (see Sec. 2.6). The final processed images in Figs. 5(d) and 5(h) were used to calculate the mean lifetime for VinTS and TSMod in cells. The mean intensity-weighted lifetime was calculated for all VinTS ($n = 94$ adhesions) and TSMod ($n = 50$ cells) samples with a mean relative intensity >0.01. These results are presented in Fig. 5(i), where the mean VinTS lifetime at the adhesion points was 2.30 ± 0.16 ns, which is significantly ($p < 10^{-6}$ by Student's t-test) longer than that of the (unloaded) TSMod (2.02 ± 0.16 ns). The conversion to apparent FRET efficiency is displayed on the right-hand axis of Fig. 5(i).

3.3 *Comparison Between Apparent* E_{FRET} *Based on FLIM and True* E_{FRET}

Given the fact that we expect to probe an ensemble of molecules corresponding to a given FRET construct and possessing a distribution of lifetimes,[33] our phase measurement conducted at a single modulation frequency corresponds to an apparent lifetime measurement, which depends on the modulation frequency that we choose. To address this, we plotted, in Fig. 6, the estimated $E_{\mathrm{FRET}}^{\mathrm{app}}$ obtained from the measured apparent lifetimes [Eq. (12)] of the soluble FRET constructs, against the published values of E_{FRET} measured independently by the sensitized emission method.[31] The published values for these constructs are $E_{\mathrm{GGS}} = 0.483$, $E_{\mathrm{TRAF}} = 0.053$, and $E_{\mathrm{TSMod}} = 0.286$.[31] We also included a zero-FRET point to account for the donor-only case. The plot demonstrates a linear relationship between the measured FRET efficiency based on the single modulation phase and the true E_{FRET} of the constructs measured independently using a sensitized emission-based method.[34] Two linear fits, with and without an intercept, are shown in Fig. 6 and suggest that the $E_{\mathrm{FRET}}^{\mathrm{app}}$ measured by FLIM is within 2% to 8% of the E_{FRET} measured by the sensitized emission method for the soluble FRET control constructs. This linear relationship, which is obtained at a given

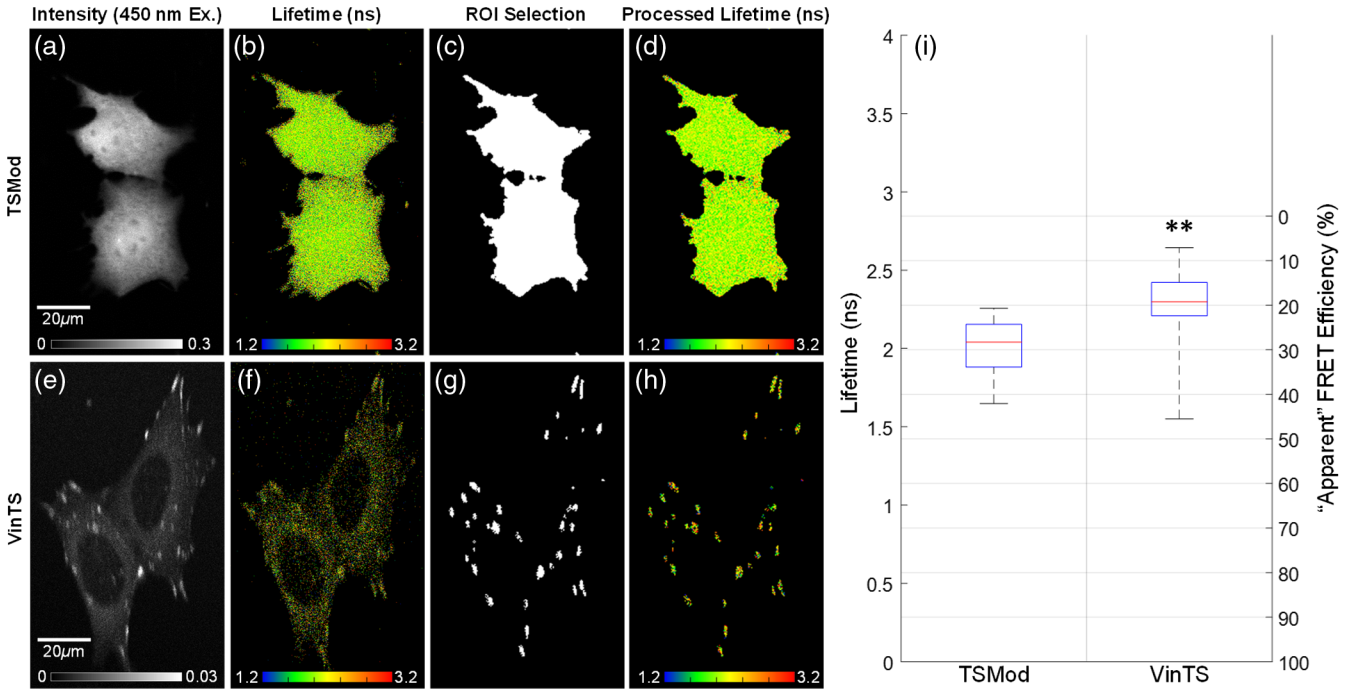

Fig. 5 Comparison of TSMod and VinTS showing cropped regions of 1024 × 1024 images (Nikon 1.3 NA 40× objective, 27.2 μs pixel dwell time). (a), (e) Representative images of the fluorescence intensity. (b), (f) Corresponding fluorescence lifetime images. (c), (g) pixel masks used for selecting the cells for TSMod and adhesions for VinTS. (d), (h) Processed images after applying the mask and 2 × 2 intensity-weighted pixel binning. (i) Box and whisker plot for lifetime (left axis) and "apparent" FRET efficiency (right axis). The asterisks denote a significant difference between the mean lifetimes of VinTS and TSMod ($p < 10^{-6}$ by Student's t-test).

modulation frequency, may be utilized as a sample-based calibration to correct for the discrepancy between the $E_{\mathrm{FRET}}^{\mathrm{app}}$ value obtained from the apparent lifetime measurement and the true FRET efficiency. For example, we can convert the average apparent $E_{\mathrm{FRET}}^{\mathrm{app}}$ of VinTS (19.28%) to its expected value given the slope of the line in Fig. 6. This results in an average E_{FRET} of 18.07% (line with intercept) or 19.49% (line without intercept) for VinTS.

4 Discussion

We have developed a two-channel FD FLIM system based on single modulation frequencies for each excitation wavelength. In this setup, the modulation waveform is a simple sinusoidal function and is fully defined by a digital waveform stored in a memory map (WFM1 MEM MAP). Other functions with harmonic frequencies may also be utilized. The system requires knowledge of the instrument-induced phase delay, which may be measured using solutions of calibration standards, such as coumarin-6 and fluorescein, with known single exponential lifetimes. The system introduced phase shift may arise from several sources including the capacitor charging time in the laser diode junction and the bias-T modulation circuit, electric and optical cable propagation delay, and phase shift in the amplifiers of the detector and digitizer circuits. In practice, this system-introduced phase shift is a constant unless the system configuration is changed, such as by changing cable length or introducing a free-space optical delay in the signal path.

To evaluate the performance of our system, we measured the apparent lifetime of mTFP1 in mTFP1-mVenus FRET standards expressed in living cells to demonstrate our ability to differentiate the short and long lifetime of mTFP1 corresponding to the FRET standards with short $(\mathrm{GGSGGS})_2$ or long (TRAF) linker, respectively (Fig. 3). These measurements are based on previous work in which such FRET standards were utilized to evaluate FLIM systems.[29,35–37] In addition, we show that the lifetime of VinTS at focal adhesions is significantly ($p < 10^{-6}$) longer than the lifetime of the unloaded TSMod probe (Fig. 5). Even under static culture conditions, cells generate large forces without being actively perturbed. Under these conditions, the vinculin tension sensor reports on the loads vinculin experiences within focal adhesions due to the force-generation capabilities of the actomyosin cytoskeleton.[10,38,39] Fluctuations in donor acceptor separation are also expected to be especially evident for tension sensors, which, unlike most two-state, on-off, FRET biosensors, are meant to measure a distribution of mechanical loads with potentially varying degrees of fluctuations as the probe is extended.[38] Thus, our ability to discern the ∼9% difference in FRET efficiency between the unloaded TSMod sensor and its loaded counterpart embedded within VinTS constitutes a markedly finer measurement than detecting the 40% difference in FRET efficiency between the soluble high (GGS) and low (TRAF) FRET standards. The current sensitivity of the system may be estimated from the standard deviation of the TSMod FRET efficiency measurements in Fig. 6, or $\Delta E_{\mathrm{FRET}} \sim \pm 5\%$. Since we expect the TSMod to be unloaded everywhere with negligible variability in the length of the linker, this standard deviation reflects our experimental error (due to both the FLIM system and biological noise), and therefore represents the current measurement uncertainty within a living cell. A 5% variance in E_{FRET} provides sufficient sensitivity to detect biologically relevant measurements typically made in mechanotransduction

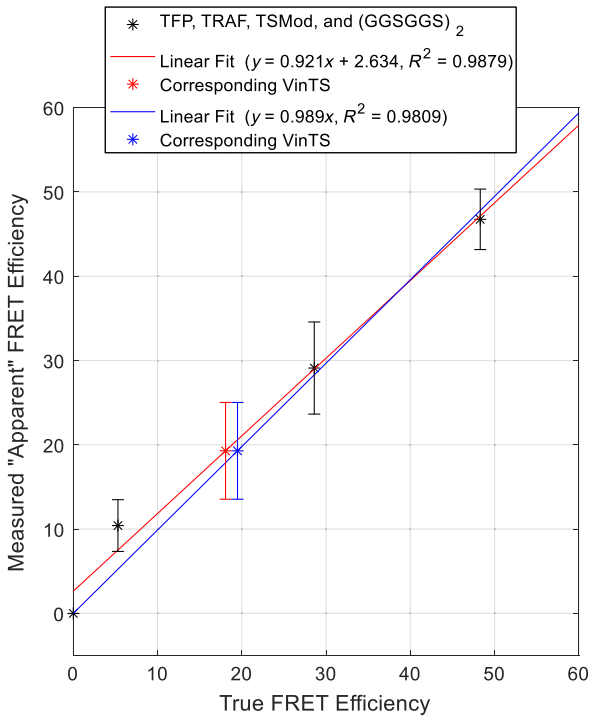

Fig. 6 Relationship between the E_{FRET}^{app} calculated from the apparent lifetime measured at a single modulation frequency (42.1875 MHz) and published E_{FRET} measured independently by the sensitized emission method. A line was fit to the data points corresponding to the soluble FRET constructs (GGS, TRAF, and TSMod), and the point at (0,0) corresponding to zero FRET efficiency (donor only). The points corresponding to VinTS were obtained by finding the true E_{FRET} for VinTS based on the slope obtained from the corresponding linear fits. Data points are mean ± standard deviation, with $n = 23$ (GGS), $n = 33$ (TRAF), $n = 50$ (TSMod), and $n = 94$ (VinTS).

experiments with E_{FRET} changes on the order of 5% to 20%.[10,38,39]

The apparent lifetime measured by our system was further converted to an "apparent" E_{FRET}^{app} value, which exhibited a linear relationship with the expected E_{FRET} for the soluble FRET constructs (Fig. 6). The slope of this line was between 0.92 and 0.99 with an R-squared value of 0.98. This suggests that the E_{FRET}^{app} measurements based on the apparent lifetime are within 1% to 8% of the expected values. *A priori*, the constructs consist of populations with multiple fluorescent lifetimes. Thus, it is not surprising that our FLIM-based E_{FRET}^{app} values are slightly different from the expected E_{FRET}. But furthermore, the linear relationship in Fig. 6 may be used as a calibration curve to convert E_{FRET}^{app} to true (expected) E_{FRET}. Applying this calibration results in an average E_{FRET} of 18% to 19.5% for VinTS and is corroborated by published FRET efficiency values for VinTS in adherent cells.[31]

By investigating the relationship between the measured signal intensity, number of emission photons, and variability in our lifetime measurements, we established that ~300 photons are required for reproducible lifetime measurements. Finally, the lifetime measurements remained within 2.9% of the initial values after continuous illumination for 120 s with a power of 25 μW at the sample. Thus, our lifetime images collected with a pixel dwell time on the order of at most tens of microseconds are largely free of photobleaching artifact. For samples expressing soluble FRET constructs with signal typically an order of magnitude higher than VinTS, we were able to achieve high-speed (128×128 images at ~9 fps) and high pixel density (2048×2048 images at ~28 s/frame) lifetime imaging using a 6.8-μs pixel dwell time. For VinTS, we used 1024×1024 with a 27.2-μs pixel dwell time.

Calculated E_{FRET}^{app} values based on apparent lifetime may be used to measure relative changes in FRET efficiency to compare experimental and control biological conditions. However, quantifying the true value of the FRET efficiency may be central to the conversion of E_{FRET} to molecular tension in pN.[10] True FRET efficiency quantification may be implemented on a standard epi-fluorescence microscope using the sensitized emission method.[31,34] This method has several drawbacks despite the fact that it might be the most straightforward way to implement FRET in a laboratory where an epi-fluorescence microscope already exists. Due to the overlap between the fluorescence excitation and emission spectra of the donor and acceptor, the FRET signal must be measured in the presence of background noise due to donor and acceptor bleedthrough in the FRET channel. In addition, normalization to fluorophore concentration as well as calibration of the instrument must be achieved in order to convert the measured raw signal to FRET efficiency.[34]

A more direct method to measure FRET relies on measuring changes in the donor's fluorescence lifetime in the presence of the acceptor (τ_{DA}), relative to the donor's lifetime in the absence of the acceptor (τ_D). In this case, the FRET efficiency is given by $E_{FRET} = 1 - (\tau_{DA}/\tau_D)$ for donor–acceptor pairs separated by a constant radius.[12] However, for most FRET constructs in which donor and acceptor pairs are connected via a flexible linker, a distribution of radii exists in the population of molecules being probed.[12,33] Therefore, this distribution gives rise to multiple fluorescence lifetimes within the molecular population being probed. To account for this in FD FLIM systems, the phase and modulation depth of the fluorescence emission are typically measured at multiple modulation frequencies and fit to equations which can account for multiexponential decays.[19] The "amplitude-weighted" average fluorescence lifetime [Eqs. (4.30) and (4.31) in Ref. 12], rather than the intensity-weighted lifetime, may then be used to calculate the average $\langle\tau_{DA}\rangle$, from which E_{FRET} may be inferred. This approach was previously validated by measuring the amplitude-weighted lifetime of high and low FRET standards similar to those used here.[37] Nonetheless, compared to measuring a single lifetime, the requirement to probe the system at multiple frequencies, followed by data fitting, lengthens data acquisition time and limits fast FLIM imaging. To enable fast lifetime image acquisition in two separate fluorescence channels, we have used in this paper a single modulation frequency for each excitation channel. A single apparent lifetime value is calculated from the relative phase delay at this modulated frequency using Eq. (12). In addition, we use here the linear relationship in Fig. 6 to calibrate the measured E_{FRET}^{app} against the true expected E_{FRET}. This calibration is effectively achieved by measuring the apparent lifetime of a few samples whose known true E_{FRET} values have been previously measured independently and becomes useful when measuring FRET samples with weak fluorescence signals often resulting in insufficient photons to fit multiexponential decay models unless a long integration time is used. This relationship can then be used to correct for the discrepancy between the apparent FRET efficiency measured at a single modulation frequency and the expected FRET efficiency. In this way, like the sensitized emission method, a single modulation FD instrument would still

require additional calibration based on known FRET samples, but it would have the significant added benefit of simplifying the FLIM instrument and allowing faster image acquisition. This is particularly advantageous in applications such as mechanobiology (or others) in which the calibration constructs are similar to the sensors and are readily available. This approach is supported here by our ability to obtain the expected FRET efficiency for the vinculin tension sensor at focal adhesions.[31] However, further validation is necessary to establish the reproducibility of this approach with other FRET sensors and corroborate the relationship found in Fig. 6. We also note that a monotonic empirical relationship between apparent and true E_{FRET} that is not linear can still be utilized as a calibration curve in our approach to convert the measured $E_{\mathrm{FRET}}^{\mathrm{app}}$ to true E_{FRET}.

Nonetheless, multiple decay times are still required in FLIM applications whose endpoints are the measurement of multiple lifetimes corresponding to different populations of the same fluorophores in different environments (e.g., free versus protein-bound NADH).[40–43] These applications still require FLIM setups with sufficient temporal resolution to allow measurement of multiple decays. FD-FLIM measurements of modulation and phase at multiple modulation frequencies also allow for robust sample characterization via the phasor plots.[42] Compared to those instruments, our system is limited to the extent that it does not currently permit measurements of multiple decay times. However, we propose that this limitation does not preclude measuring FRET efficiency and may be circumvented by utilizing the calibration curve in Fig. 6 to convert an unknown sample's apparent FRET to its corresponding true FRET efficiency. Still, the applicability of this approach beyond the initial VinTS measurement made here remains to be demonstrated. In particular, additional studies may shed more light on the nature of the relationship between apparent and true FRET efficiency observed in Fig. 6, and the potential dependence of this relationship on the choice of another modulation frequency or another fluorescent protein donor–acceptor pair.

In this study, we have used the 520-nm excitation/559-nm emission channel ("AA" channel in Fig. S6 in the Supplementary Material) to provide evidence and measurement of the acceptor (mVenus) fluorescent protein. Alternatively, a FLIM probe may be designed to have a genetically encoded nonfluorescent quencher, such as ShadowG,[44,45] so that the acceptor channel may be replaced by a different channel to view and measure the lifetime of another fluorescent marker in conjunction with the FLIM probe. It is also possible to simultaneously acquire in our system the raw "FRET channel" intensity with excitation at 450 nm and emission at 559 nm ("DA" channel, laser 1, detector 2, f_1, in Fig. S6 in the Supplementary Material). This raw FRET signal is not used for FLIM and must be corrected for acceptor and donor bleedthrough. However, this DA channel could be used to measure FRET efficiency based on the sensitized emission-based method after bleedthrough correction and proper calibration as described by Chen et al.[34] This, in turn, would allow us to calibrate the $E_{\mathrm{FRET}}^{\mathrm{app}}$ measurement from the apparent lifetime against the FRET efficiency measurement obtained by sensitized emission using the same setup.

Taken together, our results demonstrate the capabilities of a versatile scanning FLIM system that can potentially be adapted for use with a variety of FRET pairs in biological applications. We expect the simple, compact design, and optical throughput of the system, as well as its potential low-cost, to facilitate its dissemination to biological sciences labs. This in turn will advance the study of cell mechanics by allowing end-users to capitalize on the recent advancements in molecular tension probes.

Disclosures

J.P. Dumas and J. Jiang are currently employed by Thorlabs. N. Boustany and M. Pierce received consulting fees from Thorlabs Inc. Other authors have no competing interests to declare.

Acknowledgments

We gratefully acknowledge the support of Alex Cable and Thorlabs Inc. for this project. We thank Dr. B.L. Firestein and her laboratory at Rutgers for assistance with the purification of the DNA plasmids, and Dr. E. White and the Rutgers Cancer Institute of New Jersey for the iBMK cells utilized in this study. This study was partially supported by NSF Grant CMMI-1825433 to N.N.B. E.M.G. was supported by NSF graduate fellowship DGE-1644868 and Grant CMMI-1454257 to B.D.H.

References

1. C. C. DuFort, M. J. Paszek, and V. M. Weaver, "Balancing forces: architectural control of mechanotransduction," *Nat. Rev. Mol. Cell Biol.* **12**(5), 308–319 (2011).
2. D. A. Fletcher and D. Mullins, "Cell mechanics and the cytoskeleton," *Nature* **463**(7280), 485–492 (2010).
3. K. Franze, P. A. Janmey, and J. Guck, "Mechanics in neuronal development and repair," *Annu. Rev. Biomed. Eng.* **15**, 227–251 (2013).
4. M. A. Wozniak and C. S. Chen, "Mechanotransduction in development: a growing role for contractility," *Nat. Rev. Mol. Cell Biol.* **10**(1), 34–43 (2009).
5. P. Kanchanawong et al., "Nanoscale architecture of integrin-based cell adhesions," *Nature* **468**(7323), 580–584 (2010).
6. E. Spanjaard et al., "Quantitative imaging of focal adhesion dynamics and their regulation by HGF and Rap1 signaling," *Exp. Cell Res.* **330**(2), 382–397 (2015).
7. B. L. Blakely et al., "A DNA-based molecular probe for optically reporting cellular traction forces," *Nat. Methods* **11**(12), 1229–1232 (2014).
8. D. R. Stabley et al., "Visualizing mechanical tension across membrane receptors with a fluorescent sensor," *Nat. Methods* **9**(1), 64–67 (2012).
9. Y. Zhang et al., "DNA-based digital tension probes reveal integrin forces during early cell adhesion," *Nat. Commun.* **5**, 5167 (2014).
10. C. Grashoff et al., "Measuring mechanical tension across vinculin reveals regulation of focal adhesion dynamics," *Nature* **466**(7303), 263–266 (2010).
11. M. Morimatsu et al., "Molecular tension sensors report forces generated by single integrin molecules in living cells," *Nano Lett.* **13**(9), 3985–3989 (2013).
12. J. R. Lakowicz, *Principles of Fluorescence Spectroscopy*, 3rd ed., Springer, New York (2006).
13. A. Periasamy and R. N. Day, *Molecular Imaging: FRET Microscopy and Spectroscopy*, Oxford University Press, New York (2005).
14. A. Periasamy and R. M. Clegg, *FLIM Microscopy in Biology and Medicine*, CRC Press, Boca Raton, Florida (2009).
15. H. Wallrabe and A. Periasamy, "Imaging protein molecules using FRET and FLIM microscopy," *Curr. Opin. Biotechnol.* **16**(1), 19–27 (2005).
16. A. J. Bower et al., "High-speed imaging of transient metabolic dynamics using two-photon fluorescence lifetime imaging microscopy," *Optica* **5**(10), 1290–1296 (2018).
17. X. Y. Dow et al., "Video-rate two-photon excited fluorescence lifetime imaging system with interleaved digitization," *Opt. Lett.* **40**(14), 3296–3299 (2015).
18. J. Ryu et al., "Real-time visualization of two-photon fluorescence lifetime imaging microscopy using a wavelength-tunable femtosecond pulsed laser," *Biomed. Opt. Express* **9**(7), 3449–3463 (2018).
19. R. A. Colyer, C. Lee, and E. Gratton, "A novel fluorescence lifetime imaging system that optimizes photon efficiency," *Microsc. Res. Tech.* **71**(3), 201–213 (2008).

20. H. T. Chen and E. Gratton, "A practical implementation of multi-frequency widefield frequency-domain fluorescence lifetime imaging microscopy," *Microsc. Res. Tech.* **76**(3), 282–289 (2013).
21. M. Raspe et al., "siFLIMIM: single-image frequency-domain FLIM provides fast and photon-efficient lifetime data," *Nat. Methods* **13**(6), 501–504 (2016).
22. R. Franke and G. A. Holst, "Frequency-domain fluorescence lifetime imaging system (pco.flim) based on an in-pixel dual tap control CMOS image sensor," *Proc. SPIE* **9328**, 93281K (2015).
23. H. M. Wu et al., "Widefield frequency domain fluorescence lifetime imaging microscopy (FD-FLIM) for accurate measurement of oxygen gradients within microfluidic devices," *Analyst* **144**(11), 3494–3504 (2019).
24. S. Shrestha et al., "High-speed multispectral fluorescence lifetime imaging implementation for *in vivo* applications," *Opt. Lett.* **35**(15), 2558–2560 (2010).
25. M. A. Digman et al., "The phasor approach to fluorescence lifetime imaging analysis," *Biophys. J.* **94**(2), L14–L16 (2008).
26. M. J. Booth and T. Wilson, "Low-cost, frequency-domain, fluorescence lifetime confocal microscopy," *J. Microsc.* **214**, 36–42 (2004).
27. J. Tierney, C. Rader, and B. Gold, "A digital frequency synthesizer," *IEEE Trans. Audio Electroacoust.* **19**, 48–57 (1971).
28. L. A. Pipes and L. R. Harvill, *Applied Mathematics for Engineers and Physicists*, 3rd ed., McGraw-Hill, New York (1970).
29. Y. S. Sun et al., "Monitoring protein interactions in living cells with fluorescence lifetime imaging microscopy," *Methods Enzymol.* **504**, 371–391 (2012).
30. M. Y. Berezin and S. Achilefu, "Fluorescence lifetime measurements and biological imaging," *Chem. Rev.* **110**(5), 2641–2684 (2010).
31. E. M. Gates et al., "Improving quality, reproducibility, and usability of FRET-based tension sensors," *Cytometry Part A* **95**(2), 201–213 (2019).
32. R. Mathew et al., "Autophagy suppresses tumorigenesis through elimination of p62," *Cell* **137**(6), 1062–1075 (2009).
33. S. S. Vogel et al., "The impact of heterogeneity and dark acceptor states on FRET: implications for using fluorescent protein donors and acceptors," *PLoS One* **7**(11), e49593 (2012).
34. H. Chen et al., "Measurement of FRET efficiency and ratio of donor to acceptor concentration in living cells," *Biophys. J.* **91**(5), L39–L41 (2006).
35. C. Thaler et al., "Quantitative multiphoton spectral imaging and its use for measuring resonance energy transfer," *Biophys. J.* **89**(4), 2736–2749 (2005).
36. S. V. Koushik et al., "Cerulean, Venus, and $Venus_{Y67C}$ FRET reference standards," *Biophys. J.* **91**(12), L99–L101 (2006).
37. R. N. Day, "Measuring protein interactions using Forster resonance energy transfer and fluorescence lifetime imaging microscopy," *Methods* **66**(2), 200–207 (2014).
38. A. S. LaCroix et al., "Tunable molecular tension sensors reveal extension-based control of vinculin loading," *Elife* **7**, e33927 (2018).
39. K. E. Rothenberg et al., "Vinculin force-sensitive dynamics at focal adhesions enable effective directed cell migration," *Biophys. J.* **114**(7), 1680–1694 (2018).
40. J. R. Lakowicz et al., "Fluorescence lifetime imaging of free and protein-bound NADH," *Proc. Natl. Acad. Sci. U. S. A.* **89**(4), 1271–1275 (1992).
41. M. C. Skala et al., "In vivo multiphoton fluorescence lifetime imaging of protein-bound and free nicotinamide adenine dinucleotide in normal and precancerous epithelia," *J. Biomed. Opt.* **12**(2), 024014 (2007).
42. C. Stringari et al., "Phasor fluorescence lifetime microscopy of free and protein-bound NADH reveals neural stem cell differentiation potential," *PLoS One* **7**(11), e48014 (2012).
43. H. Wallrabe et al., "Segmented cell analyses to measure redox states of autofluorescent NAD(P)H, FAD & Trp in cancer cells by FLIM," *Sci. Rep.* **8**, 79 (2018).
44. H. Murakoshi et al., "A dark green fluorescent protein as an acceptor for measurement of Forster resonance energy transfer," *Sci. Rep.* **5**, 15334 (2015).
45. P. Ringer et al., "Multiplexing molecular tension sensors reveals piconewton force gradient across talin-1," *Nat. Methods* **14**(11), 1090–1096 (2017).

John-Paul Dumas attended Union College, New York, from 2010 to 2014 where he earned his BS degree in bioengineering. In 2014, he joined the PhD program at Rutgers University in the Biomedical Engineering Department. He worked under Professor Mark Pierce with a research focus on biomedical optics and imaging. He graduated from Rutgers in 2019 and is currently working at Thorlabs, Inc. as a technical marketer specializing in life science and imaging products.

James Y. Jiang received his BS degrees in applied physics and in computer science in 1997, and his PhD in optics in 2002, all from Shanghai Jiao Tong University. He joined Beckman Laser Institute, University of California, Irvine as a postdoctoral researcher in 2003 and focused on second harmonic OCT microscopy and high-resolution OCT research projects. In 2005, he joined Thorlabs Inc. as a researcher focusing on the research and development of novel laser imaging systems for biomedical and industrial applications.

Evan M. Gates is a PhD candidate in biomedical engineering at Duke University. He received a BS degree in both mechanical and biomedical engineering from Carnegie Mellon University, and he was the recipient of a National Science Foundation Graduate Research Fellowship. His research focuses on using molecular tension sensors to study force-transmission during fundamental multicellular processes such as collective cell migration.

Brenton D. Hoffman received his PhD in chemical and biomolecular engineering from the University of Pennsylvania and then completed postdoctoral training within the Cardiovascular Research Center at the University of Virginia. Since 2012, he has been an assistant professor within the Biomedical Engineering Department at Duke University. His work is focused on the development, creation, and use of optically-based molecular tension sensors for the study of biophysics, cell biology, and mechanosensitive disease states.

Mark C. Pierce is an associate professor of biomedical engineering at Rutgers University. His lab focuses on development and translation of multiscale optical imaging modalities for clinical and basic science applications. He received his PhD from the University of Manchester (UK) and completed postdoctoral training at Massachusetts General Hospital and Rice University.

Nada N. Boustany is an associate professor of biomedical engineering at Rutgers University. Her lab develops quantitative imaging methods with applications in biophysics and cell biology. She received her PhD from the Harvard-MIT Division of Health Sciences and Technology and conducted postdoctoral work in bioengineering at Johns Hopkins University.